Optimal observing strategies for velocity-suppressed dark matter annihilation

Nolan Smyth,[*] Gabriela Huckabee,[†] and Stefano Profumo[‡]

Department of Physics, University of California, Santa Cruz, 1156 High Street, Santa Cruz, California 95064, USA and Santa Cruz Institute for Particle Physics, 1156 High Street, Santa Cruz, California 95064, USA

(Received 11 May 2021; accepted 18 October 2021; published 1 December 2021)

Numerous particle models for the cosmological dark matter feature a pair-annihilation rate that scales with powers of the relative velocity between the annihilating particles. As a result, the annihilation rate in the central regions of a dark matter halo can be significantly lower than at the halo's periphery for particular ambient gravitational potentials. While this might be offset by an increasing dark matter pair number density in the inner halo, it raises the question; what angular region for dark matter models with velocity-suppressed annihilation rates optimizes the signal to noise ratio? Here, we consider simplified background models for galactic and extragalactic targets and demonstrate that the optimal observing strategy varies greatly case by case. Generally, a bright central source warrants an annular region of interest, while a flatter background warrants as large as possible an angular region, possibly including the central regions.

DOI: 10.1103/PhysRevD.104.123003

I. INTRODUCTION

The production of Standard Model particles from the annihilation of dark matter (DM) particles provides a detectable signal with which to indirectly probe DM models (for reviews, see e.g., [1–3]). Dwarf spheroidal galaxies (dSphs) are of particular interest in indirect detection searches as they are generally DM dominated and have a low astrophysical foreground [4]. Other prime targets are the Galactic Center (GC) region and nearby galaxies such as M31 [5,6] and M87 [2,3,7].

The total photon flux from a specific astrophysical object due to DM annihilation is proportional to that object's *J-factor*, also sometimes called the *astrophysical factor*. The J-factor is determined by the astrophysical properties of the object, such as its DM density profile. In calculating the predicted photon flux from DM annihilation, often one assumes a velocity-independent cross section, which, in turn, implies a velocity-independent J-factor. However, in cases where the velocity-independent s-wave channel is subdominant to the velocity-dependent p-wave and d-wave channels, the J-factor must effectively include the velocity-dependent contribution from the cross section. As shown by [8], in the general case of a velocity-dependent cross section, the J-factor scales as the moments of the DM velocity distribution. They show that even in this general case, the J-factor is strongly correlated with the DM density and weakly correlated with the velocity dispersion.

However, we show in this work that for simple cases of p-wave and d-wave dominated annihilation, the velocity-dependent J-factor implies that the optimal signal to noise ratio is generally achieved for a different observation strategy than in the velocity-independent, s-wave dominated case. For example, we find an annular field of view to be superior to a disk when the background gamma-ray signal is sharply peaked at the center of a DM halo. This is due to two factors. First, the velocity distribution of DM particles is peaked off center in the halo, resulting in a boost to the velocity-dependent J-factor in this region. Second, the benefits of including the high-density region at the center of the halo in the J-factor are outweighed by the detriment of a large background.

In this study we consider two broad classes of observational targets: (1) a generic extragalactic target, and (2) the Milky Way Galactic Center. The latter has been the subject of much debate due to the extended gamma-ray excess within the inner region of the bulge [9,10]. Annihilating dark matter may be responsible for this excess and is the focus of this paper, but unresolved gamma-ray pulsars and other faint baryonic sources have also been put forth as viable explanations [11–14]. The extragalactic class, which includes nearby galaxies such as M31, M87, and M33, is of interest because the central bulge and stellar disk are resolvable as two distinct components; something that is not possible in the Milky Way Galactic Center due to bright disk contamination. We include in this category local dwarf spheroidal galaxies (dSphs), satellites of the

[*]nwsmyth@ucsc.edu
[†]ghuckabe@ucsc.edu
[‡]profumo@ucsc.edu

Milky Way, as the angular extent of these satellites is quite similar to nearby galaxies in the Local Group. This set of nearby galaxies and satellites has ideal conditions for the observation of DM annihilation and has been the subject of extensive theoretical and observational study [15–18].

This paper is organized as follows. In Sec. II we summarize different scenarios in which p-wave and d-wave annihilation processes are dominant or comparable to s-wave channels. In Sec. III we detail our approach and methodology. In Sec. IV we present our findings. Lastly, we discuss the implications of our results in Sec. V.

II. VELOCITY-DEPENDENT CROSS SECTIONS

We are interested in models in which the DM annihilation cross section has a nontrivial velocity dependence. In a model-independent approach, we parameterize this dependence as

$$\langle \sigma_A v_{\rm rel} \rangle = \langle \sigma_A v_{\rm rel} \rangle_0 \left(\frac{v_{\rm rel}}{c} \right)^n. \tag{1}$$

where σ_A is the annihilation cross section and $\langle \sigma_A v_{\rm rel} \rangle_0$ is the velocity-independent piece of the thermally-averaged cross section.

We aim to keep our approach as general as possible, but we will primarily consider three cases for illustrative purposes:

(1) $n = 0$: This is the s-wave channel, which is the typical case of a velocity-independent cross section.
(2) $n = 2$: The p-wave channel, which is relevant in particular models such as Majorana fermion DM annihilating into fermion/antifermion pairs. In this scenario, the s-wave channel is chirality suppressed and so p-wave annihilation is dominant [19].
(3) $n = 4$: This is the d-wave channel, which becomes relevant in the case of real scalar singlet DM annihilating into lepton/antilepton pairs [20]. Again, the s-wave channel is chirality suppressed and now the p-wave channel requires a CP-odd bilinear involving two real scalars, for which there is no such operator. Similarly, for the case of scalar DM annihilation into a pair of massless gauge bosons, the cross section is also d-wave suppressed [21].

Sommerfeld enhancement ($n = -1$) is also a well-motivated case, but will tend to enhance the J-factor towards the center of a DM halo where the typical velocity is lower. We do not expect this case to yield a significantly different optimal observing strategy from the benchmark s-wave case. Additionally, it is possible to have linear velocity suppression (i.e., $n = 1$) for dark matter models with final-state phase-space suppression (see e.g., [22]). However, we do not expect qualitatively different behavior compared to other velocity-dependent channels. As such, we will exclusively focus on the three aforementioned cases of s, p, and d-wave annihilation.

III. FORMALISM

A. Velocity-dependent J-factor

The dark matter annihilation signal is proportional to the square of the DM density integrated over the line of sight. The literature refers to this integral as the J-factor, also called the astrophysical factor. In the velocity-independent case, it can be understood as a measure of how many DM pairs exist between an observer and their observation target. In the more general case, a velocity dependence can appear through the cross section, and the appropriate J-factor, which we indicate with the symbol $\mathcal{J}$, is defined as

$$\mathcal{J} = \int dl \frac{\langle \sigma_A v_{\rm rel} \rangle}{(\sigma_A v_{\rm rel})_0} \rho(r)^2, \tag{2}$$

where ρ is the DM density. Parametrizing the velocity-dependent annihilation cross section as in (1), the J-factor scales as the moments of the dark matter velocity [8].

$$\mathcal{J} = \int dl \rho(r)^2 \left(\frac{\mu_n(r)}{c^n} \right), \tag{3}$$

where $\mu_n = \int d^3 v_{\rm rel} f(v_{\rm rel}) v_{\rm rel}^n$ is the nth moment of the velocity distribution.

We assume that the dark matter follows a Maxwell-Boltzmann distribution

$$f(\mathbf{v}) \propto (\sigma_v^2)^{-3/2} e^{-v^2/\sigma_v^2}, \tag{4}$$

where the velocity dispersion is $\sigma_v^2 = \frac{\langle v^2 \rangle}{3}$ from the equipartition theorem. Under the assumption of a virialized halo, the average kinetic energy of a dark matter particle is proportional to the average gravitational potential energy, $[\langle \frac{1}{2} m v^2 \rangle = \langle \frac{1}{2} \frac{GM(<r)}{r} \rangle]$. In this case, we can take $\langle v^2 \rangle$ to be proportional to the square of the circular velocity at a given radius,

$$v_c(r) = \sqrt{\frac{2GM(<r)}{r}}. \tag{5}$$

Using the fact that the dark matter velocities are uncorrelated for an isotropic Maxwell-Boltzmann distribution, it is straightforward to show that the average relative velocity of two dark matter particles of identical mass is given by

$$\begin{aligned} \langle v_{\rm rel}^2 \rangle &= \langle (\mathbf{v} - \mathbf{v}')^2 \rangle \\ &= \int d^3\mathbf{v} \int d^3\mathbf{v}' (\mathbf{v} - \mathbf{v}')^2 f(\mathbf{v}) f(\mathbf{v}') = 2\langle v^2 \rangle = 2v_c^2. \end{aligned} \tag{6}$$

For the purposes of this paper, we will consider two cases for the DM density; a "cuspy" Navarro-Frenk-White

(NFW) profile and a "cored" Burkert profile [23–25]. Note that once we specify the density profile, the velocity is fully determined in this simple model, in which we neglect the gravitational potential of baryons. The NFW profile is given by [23]

$$\rho(r) = \frac{\rho_0}{(\frac{r}{r_s})(1+\frac{r}{r_s})^2}. \tag{7}$$

The mass enclosed in a sphere of radius r centered on a halo with an NFW density profile is

$$M(<r) = 4\pi\rho_0 r_s^3\left(\frac{r_s}{r_s+r} - 1 + \log\left(1+\frac{r}{r_s}\right)\right). \tag{8}$$

The calculation for the Burkert profile is analogous. Plugging (8) into (5), we have everything we need to calculate the velocity-dependent J-factor.

B. J-factor calculation

Assuming a particular density profile, the DM velocity is known at all locations under the assumptions outlined in Sec. III A. We can therefore perform the line of sight integral to calculate the J-factor per unit solid angle as a function of the angle b, which is measured with respect to the center of the target halo as shown in Fig. 1.

Expressing the distance to the center of a DM halo in terms of the distance from the solar neighborhood, we have

$$r = \sqrt{r_d^2 - 2lr_d\cos(b) + l^2}, \tag{9}$$

where r_d is the distance between the Sun and the center of the DM halo and l is the distance from the Sun and the point of evaluation. We then calculate the J-factor for a range of discrete values for b from 0 out to a maximum angle $b_{\max} = \arctan(\frac{r_t}{r_d})$, corresponding to a line tangent to the edge of the halo as defined by the tidal radius r_t. We interpolate between these points to get $\mathcal{J}(b)$.

Because the ratio r_s/r_d is nearly identical for M31, M87, and dSphs such as Draco, the angular scale of these halos is quite similar. We will therefore categorize all such halos as an extragalactic (EG) source case study. Note that we do not necessarily expect the shape of the DM distribution to be identical in each of these halos, but it is not necessary to separate these cases further for the illustrative purposes of this work. Thus for the EG case, we use model values corresponding to the dSph Draco: $\rho_0 = 2.3\times10^8\, M_\odot\,\mathrm{kpc}^{-3}$, $r_d = 76$ kpc, $r_t = 0.97$ kpc, and $r_s = 0.35$ kpc as calculated in [26]. For the Galactic Center, we use $\rho_0 = 4.9\times10^6\, M_\odot\,\mathrm{kpc}^{-3}$, $r_d = 8$ kpc, $r_t = 90$ kpc, and $r_s = 15.3$ kpc.

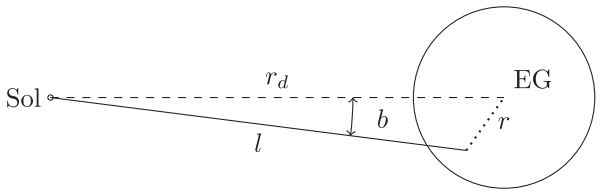

FIG. 1. Geometric parameters used in J-factor calculation. EG is a generic extragalactic body that hosts DM; r_d is the displacement between our star, Sol, and the center of EG; l is the displacment between Sol and a point in EG's DM halo; b is the angle made between r_d and l; and r is the radial distance from the center of EG.

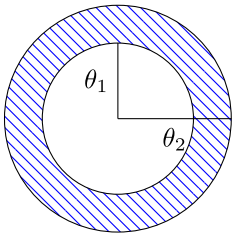

FIG. 2. The shaded annulus region is the area in which we evaluate the signal to noise ratio.

To determine the total J-factor for a particular solid angle field of view, we integrate the J-factor over all relevant angles, as shown in Fig. 2. For an annulus centered at $b = 0$, making use of the spherical symmetry of the halo, the total J-factor is

$$2\pi\int_{\theta_1}^{\theta_2}\mathcal{J}(b)bdb. \tag{10}$$

C. Gamma-ray background

One of the challenges in conclusively detecting a signal from dark matter annihilation is that the signal must be distinguishable from the astrophysical background. At gamma-ray energies, key sources of background include inelastic cosmic-ray interactions with ionized gas and inverse Compton scattering of high-energy electrons off of the intervening photon background. Gamma-ray point sources within or beyond the halo of interest contribute additional noise.

There are certain characteristics of DM annihilation that may make it distinguishable from the astrophysical background. In addition to model-dependent spectral features, DM annihilation is expected to result in a signal that is highly concentrated towards the central regions of the halo, but still more extended than a point source. In order to extract a potential signal, it is paramount to identify the optimal observation region, which, we define here as the region with the largest signal to noise ratio.

Regarding gamma-ray sources within the DM halos of interest, studies using data from the Fermi Large Area Telescope (LAT) have shown that no statistically significant excess of gamma-ray emission is present in eight observed dSph candidates [27]. However, in larger galaxies, a

significant gamma-ray background from the central regions of the halo has been detected. See, for instance, promising targets for DM searches such as the M31 (Andromeda) galaxy, where a central diffuse emission has been detected [5,28]; in other cases, the background source is genuinely a pointlike object, such as an active galactic nucleus as in the case of M87 [29].

For simplicity, we assume a model of gamma-ray background consisting of two components. For the extragalactic case study, we use (1) an isotropic component, modeling the diffuse background, and (2) a central point source, suitably smeared to account for the finite instrumental point spread function (see details below). The isotropic piece is aimed at capturing both the diffuse gamma-ray background produced by interactions of high-energy cosmic rays with interstellar gas, and the extragalactic gamma-ray background. The point source accounts for the contribution from gamma-ray emission in the central region of galaxies from active galactic nuclei or other sources, such as a dense population of unresolved millisecond pulsars [30,31].

We model the contribution from the point source as a Gaussian centered at the center of the given DM halo ($b = 0$). The photon count from this component of the background is proportional to

$$N_G(b) \propto \frac{1}{\sigma\sqrt{2\pi}} e^{-\frac{1}{2}\left(\frac{b^2}{\sigma^2}\right)}, \tag{11}$$

such that σ is the angular width of the central source accounting for the instrument-dependent point spread function. We define $N_G(b)$ as the contribution from the entire line of sight for a given angle b so that the total background from the point source is integrated over the field of view

$$N_{G\mathrm{tot}} \propto \int_{\theta_1}^{\theta_2} N_G(b) b db. \tag{12}$$

The total isotropic contribution to the background is simply proportional to the field of view

$$N_{I\mathrm{tot}} \propto N_{I0}(\theta_2^2 - \theta_1^2), \tag{13}$$

where N_{I0} is the isotropic background per solid angle. Thus the total background contribution is simply $N_{I\mathrm{tot}} + N_{G\mathrm{tot}}$.

We normalize the isotropic background relative to the area of the Gaussian point source (i.e., 1) so that $N_{G\mathrm{tot}} = \eta N_{I0}$, in which η can take on a range of values. For the Galactic Center case, we normalize the bulge component of the background relative to the point source, such that $N_{G\mathrm{tot}} = \eta N_B(0)$. For the Galactic Center, the total background is thus $N_{B\mathrm{tot}} + N_{G\mathrm{tot}}$, where $N_{B\mathrm{tot}} \propto \int_{\theta_1}^{\theta_2} N_B(b) b db$.

A large η corresponds to the case where the central gamma-ray source dominates the background, such as in the case of galaxies with an active galactic nucleus. Conversely, a smaller η corresponds to a smaller contribution from the central region of a halo and a flatter background profile. This is most relevant for dSphs where there is not typically a large central gamma-ray source, but a subdominant faint source below detection threshold cannot be ruled out (see e.g., [32]).

The number of detected photons amounts to counting independent events that randomly occur at a constant rate, and is therefore well described by a Poisson distribution. Since the mean value of a Poisson distribution is also its variance, the standard deviation is simply the square root of the count. We therefore take the noise to be given by the square root of the number of background gamma-ray events. Therefore, we define the optimal observing region as the region that maximizes the quantity

$$\frac{\mathcal{J}}{N_{\mathrm{tot}}^{1/2}}. \tag{14}$$

For the Galactic Center, the diffuse gamma-ray emission is a complex superposition of a variety of sources, including the isotropic gamma-ray background, resolved and unresolved point sources, and emission from neutral pion decay, inverse Compton scattering, and bremsstrahlung. We therefore do not attempt to simplify the background morphology, and instead utilize data-driven background models employed by the Fermi-LAT Collaboration in their analysis of the GC region. Specifically, we choose to employ background model ${}^{S}\mathrm{S}^{Z}4^{R}20^{T}150^{C}5$ (see [33] for a detailed model description) in the $-5° \leq b \leq 5°$ Galactic-latitudinal window (Fig. 21, top-left panel in [33]) and the same model, in the longitudinal window $-30° \leq l \leq 30°$ (Fig. 20, middle panel). The relative normalization of the signal and of the background does not affect the determination of the optimal observing region in any case.

IV. RESULTS

A. Extragalactic source

For the extragalactic case, we show $\mathcal{J}(b)$ per unit solid angle for s-wave, p-wave, and d-wave annihilation in Fig. 3. Note that due to the assumption of the halo's spherical symmetry, $\mathcal{J}$ is only a function of one variable, the angle b.

In the s-wave case, the J-factor per unit solid angle decreases rapidly with increasing b, decreasing approximately to 90% from $b = 0.001$ to $b = 0.01$ degrees. By comparison, the p- and d-wave channels decrease at more modest rates and contribute significantly to the J-factor out to larger angles. This is because velocity increases as a function of r, the distance from the center of the halo, up until $r \approx r_t$ at which point the DM particles are tidally stripped away and the enclosed mass ceases to increase. Thus, the line of sight integral through the halo will be

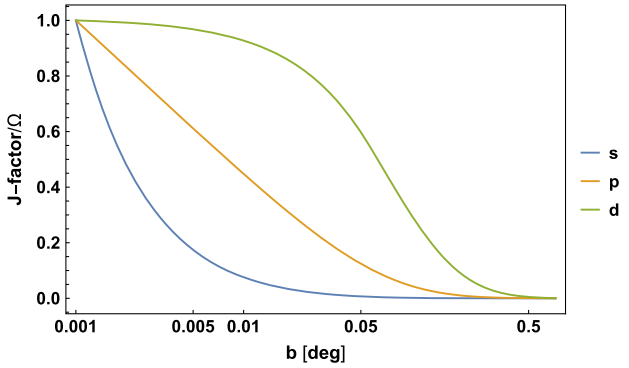

FIG. 3. $\mathcal{J}$ per solid angle as a function of the angle b for different annihilation channels, normalized to their respective values at $b = 10^{-3}$ degrees. The contribution to the J-factor from the velocity-dependent p- and d-wave channels extends to larger angles when compared to the velocity-independent s-wave case.

enhanced when including this higher velocity region due to the velocity dependence of the cross section. Because the noise grows as the square root of the background, there must be a significant enhancement of $\mathcal{J}$ or a large spike in the background signal at small b in order for it to be prudent to exclude the central region from the region of interest. We note that there are uncertainties associated with the calculation of the tidal radius. However, only a small fraction of the total annihilation flux comes from the outermost regions of the halo, so we do not expect changes in the tidal radius to affect our results in any meaningful way (see the discussion in [26] for more details).

We plot $\frac{\mathcal{J}}{N_b^{1/2}}$ as a function of θ_1 and $\theta_2 - \theta_1$, the angular extent of the inner side of the annulus and the thickness of the annulus, respectively. Using an NFW density profile for Draco, we show the signal to noise ratio for a dominant central gamma-ray source ($\eta = 20$) for the case of s-wave, p-wave, and d-wave annihilation in Fig. 4. We see that for the s-wave channel, the optimal strategy is a large circular field of view, including the entire angular extent of the source. For the p-wave case, there is a much broader range of observation strategies that yield large signal to noise ratios; the disk field of view is still viable, but excluding the central region yields a similar outcome. However, for the d-wave case, the optimal observation strategy becomes an annulus, excluding the inner 0.1 degrees of the halo and having a slightly smaller field of view, with a width extending only about 0.3 degrees, i.e., cropping out both the inner and outer regions of the halo.

For reference, the dots shown on the EG figures represent the observation strategies used in previous searches for gamma-ray emission due to dark matter annihilation. The black dot corresponds to surveys of Milky Way dSphs using Fermi-LAT data [18,34]. The orange and yellow dots correspond to observations of M31, again using Fermi-LAT [15,16]. We note that a square field of view (e.g., $10° \times 10°$) is represented as a circular field of view (e.g., $\theta_2 - \theta_1 = 10°$) in the figure for ease of comparison.

It is also worth keeping in mind that the angular resolution of Fermi-LAT varies depending on the single-photon energy. For > 10 GeV photons, the resolution is $< 0.15°$, whereas for sub-GeV photons, the resolution is $\gtrsim 1.0°$. The typical energy range observed is $\approx$100 MeV–500 GeV. For comparison, next generation telescopes, such as AdEPT, should achieve 0.1° at $\approx$1 GeV [35]. We see that even with current-generation instruments, there is room for improvement in terms of the signal-to-noise ratio for the given astrophysical background.

Using the cored Burkert density profile,

$$\rho_c = \frac{\rho_0}{(1 + \frac{r}{r_s})(1 + (\frac{r}{r_s})^2)}, \tag{15}$$

we show the signal to noise ratio in Fig. 5 for s- and p-wave channels. The behavior of the d-wave channel in this case is quite similar to that of the p-wave channel so we only show s and p for simplicity. The width of the central point source is fixed at $\sigma = 0.05$ degrees. Similarly to the corresponding NFW profile examples, the best field of view for the velocity-independent channel is either a disk or a thin

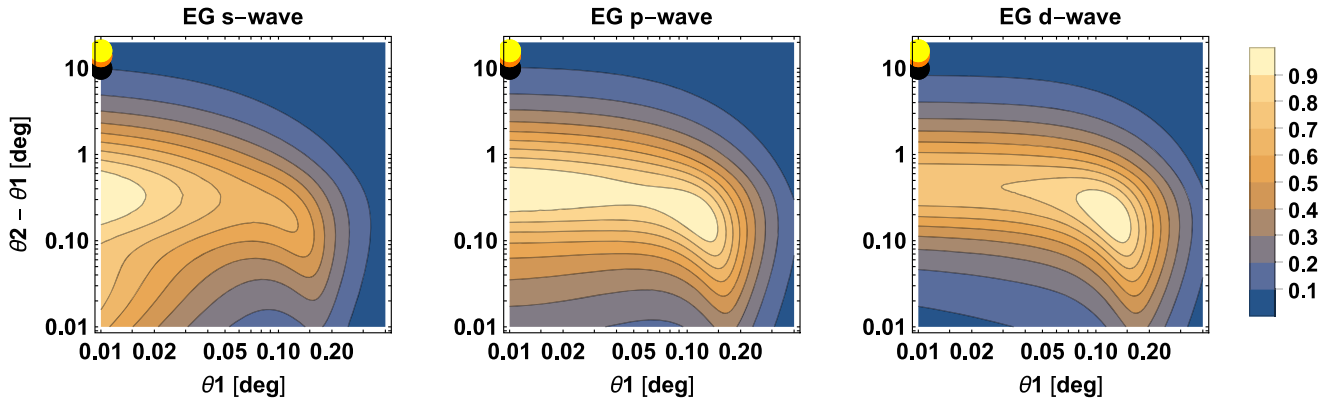

FIG. 4. $\frac{\mathcal{J}}{N_{\rm tot}^{1/2}}$ for s-, p-, and d-wave annihilation for an extragalactic source using an NFW density profile with $\sigma = 0.05°$ and $\eta = 20$. The black dot is the field of view used in a Fermi-LAT survey of Milky Way (MW) satellites [18,34], while the orange and yellow dots correspond to observations of M31 using Fermi-LAT [15,16].

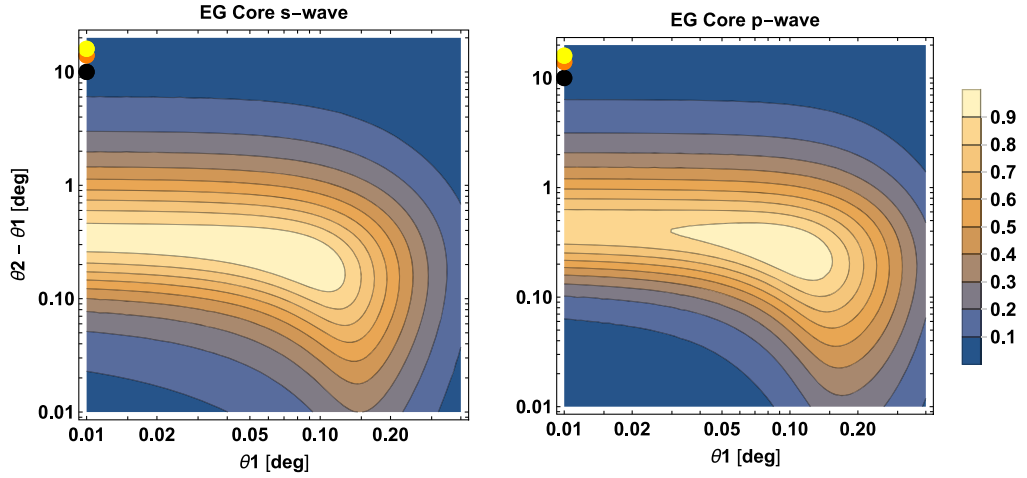

FIG. 5. $\frac{\mathcal{J}}{N_{\rm tot}^{1/2}}$ for s- and p-wave annihilation for an extragalactic source using a Burkert profile with $\sigma = 0.05°$ and $\eta = 3$. The black dot is the field of view used in a Fermi-LAT survey of MW satellites [18,34], while the orange and yellow dots correspond to observations of M31 using Fermi-LAT [15,16].

annulus. For the velocity-dependent channels, the optimal field of view is achieved with an annulus, excluding the inner 0.05 degrees of the halo, which corresponds to the width of the point source. Note that the point source need not be extremely bright for this to be the case; this behavior occurs for a moderate value of $\eta = 3$. The extent of the annulus is only about 0.4 degrees, whereas the total extent of sources like M31, M87, and Draco are about 0.7 degrees, so excluding the outermost region of these halos would be beneficial.

B. Galactic Center

We calculate $\frac{\mathcal{J}}{N_{\rm b}^{1/2}}$ for the Galactic Center for s-, p- and d-wave annihilation for the ${}^{S}\mathrm{S}^{Z}4^{R}20^{T}150^{C}5$ background model, utilizing its longitudinal (Fig. 6) and latitudinal (Fig. 7) profile as calculated by the Fermi-LAT Collaboration in Ref. [33]. The dots shown in the GC figures represent the observation strategies used in previous gamma-ray surveys in the Galactic Center. The red dot represents a survey using Fermi-LAT data for energies 2 GeV—20 GeV with a $< 2°$ plane mask with respect to the Galactic latitude [36]. For ease of comparison, we represent this as a circular 2° mask in the figures. The green dot corresponds to a search for p-wave annihilation of dark matter using Fermi-LAT in the energy range 10 GeV—600 GeV [37,38]. The region of interest was $2° \times 2°$, approximately represented in the figure as $\theta_2 - \theta_1 = 2°$.

Our findings indicate that:

(i) in the case of s-wave annihilation the optimal observing strategy, optimizing signal to noise for the actual gamma-ray background in the Galactic

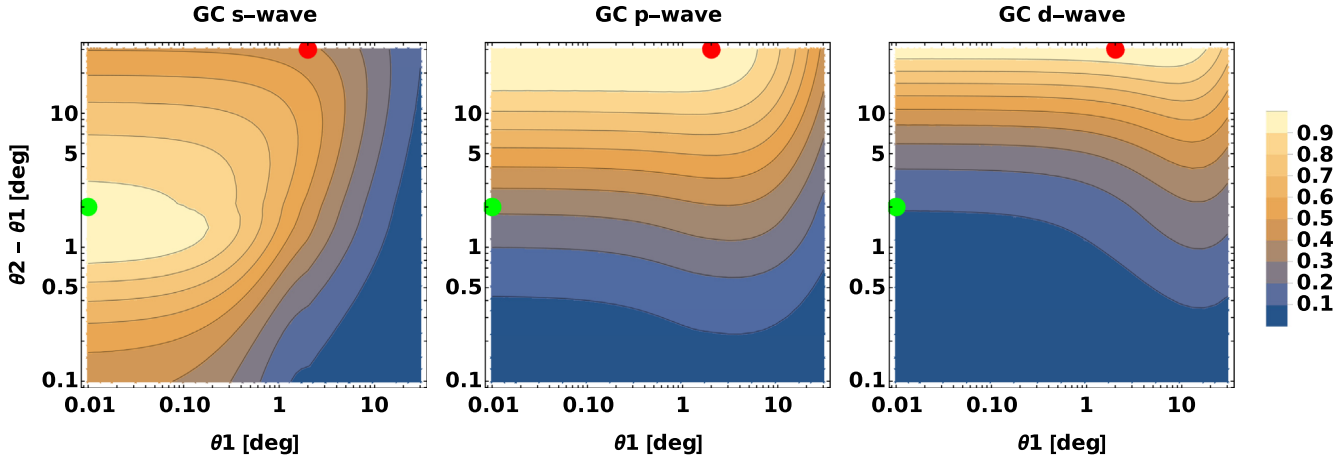

FIG. 6. $\frac{\mathcal{J}}{N_{\rm tot}^{1/2}}$ for s-, p-, and d-wave annihilation in the Galactic Center with Fermi-LAT background model ${}^{S}\mathrm{S}^{Z}4^{R}20^{T}150^{C}5$ in the $-5° \leq b \leq 5°$ Galactic longitudinal window [33] (Fig. 21, top-left panel). The green dot is the field of view used by a Fermi-LAT survey of the Galactic Center looking for p-wave annihilation [37,38]. The red dot corresponds to a search for s-wave annihilation using Fermi-LAT with a two degree plane mask [36].

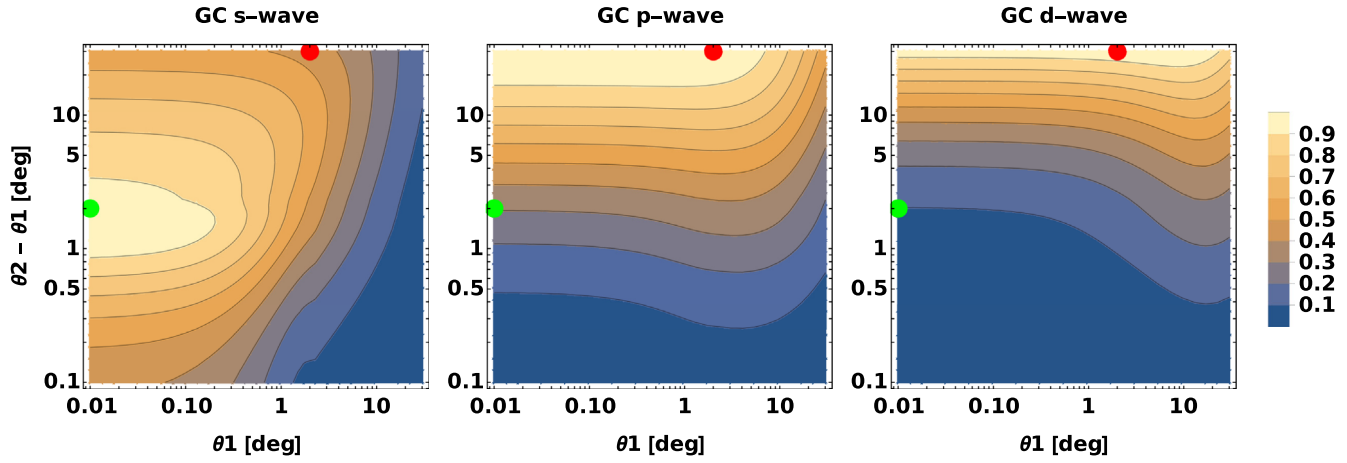

FIG. 7. $\frac{\mathcal{J}}{N_{\rm tot}^{1/2}}$ for s-, p-, and d-wave annihilation in the Galactic Center with Fermi-LAT background model ${}^{S}\mathrm{S}^{Z}4^{R}20^{T}150^{C}5$ in the latitudinal window $-30° \leq l \leq 30°$ [33] (Fig. 20, middle panel). The green dot is the field of view used by a Fermi-LAT survey of the Galactic Center looking for p-wave annihilation [37,38]. The red dot corresponds to a search for s-wave annihilation using Fermi-LAT with a two degree plane mask [36].

center corresponds to a few-degree window with $\theta_1 \simeq 0$ and $1° \lesssim \theta_2 \lesssim 3°$; this holds for both the latitudinal and longitudinal background models, and is thus expected to be a rather generic finding for the GC region.

(ii) in the p-wave case, we find that the optimal observing strategy calls for $0 \lesssim \theta_1 \simeq 7°$, and a large value of θ_2; the d-wave result is similar, with a preference for even larger values of both θ_1 and θ_2—again, the result holds for both GC background models. This is because the velocity enhancement of the cross section leads to a non-negligible contribution to the J-factor per solid angle, even far from the Galactic Center.

(iii) we find that previous analyses for s- and p-wave signals did not pursue optimal observing strategy (interestingly, we find that the p-wave search was optimal for s-wave annihilation models, and vice versa). However, we note that in the case of the p-wave search the corresponding survey considered the existence of a localized dark matter over density near Sag A^*, which could significantly change the J-factor [38,39]. We did not consider DM substructures in this work, so we leave this possibility to future investigation.

V. DISCUSSION AND CONCLUSIONS

In this paper, we have investigated the behavior of the DM annihilation rate through its dependence on the J-factor for cases in which the annihilation cross section is velocity dependent. Under simple assumptions for the astrophysical background, we find that the annihilation signal to noise ratio can be larger for an annulus field of view than for a disk when considering p- and d-wave channels, even when there is not an overwhelming background from a central gamma-ray point source. This can be true for the extragalactic case, regardless of whether the DM distribution is cuspy or cored. In the case of the Galactic Center, the optimal observation strategy for velocity-dependent channels is again quite different than for the velocity-independent one, but this manifests differently than in the extragalactic scenario. Here, we find that the p-wave signal to noise ratio is optimized for a much larger field of view than that of the s-wave signal. Intriguingly, one can search for both channels simultaneously and still have a very high signal to noise ratio for each by masking the inner 1–5 degrees of the halo and extending the field of view out to nearly 100 degrees.

We have taken a number of simplifying assumptions throughout this paper for illustrative purposes. It is now worthwhile to mention and revisit these assumptions. We have neglected the baryonic matter contribution to the gravitational potential, which would contribute to the DM velocity dispersion (this is expected to be a subdominant effect in some cases, for instance dSph, but more relevant in others, such as the Galactic Center). We have also ignored the possibility of DM substructure within the Milky Way and extragalactic halos. Such substructures would alter both the density and the velocity distribution of the dark matter, and therefore would extend beyond our analysis.

Another simplifying assumption was that the DM relative velocity distribution follows a Maxwell-Boltzmann distribution. In reality, this is an oversimplification as the distribution is only truly Maxwell-Boltzmann for the case of a singular isothermal sphere. More generally, one could consider an anisotropic distribution and relate the DM velocity distribution to the density profile through the Eddington inversion formula [40]. In this case, the velocity dispersion would no longer be trivially related to the circular velocity and one would need to more accurately determine the relative velocity of the dark matter particles to calculate $\mathcal{J}$.

Specific values for the width of the central gamma-ray point source σ and the relative normalization of the background sources η were chosen *ad hoc* on the basis that these served as reasonable benchmarks and demonstrated nontrivial results for various annihilation channels. The purpose of this more general work was to demonstrate how one might carry out such an analysis and to demonstrate a few interesting cases as examples. Ideally, one would analyze a given target of observation and determine the optimal strategy for that particular target using the approach and method presented here.

We have examined both an NFW and core-type Burkert density profile for the dark matter. In reality, the density distribution of DM halos is wide ranging [for the case of dSph see e.g., 41]. As a result, the optimal observational strategy for different dSphs may vary, even for the same annihilation channel and similar central gamma-ray sources.

Since the annihilation signal scales everywhere proportionally to the annihilation rate, our results hold independent of the signal strength. Given the schematic assumptions for "extragalactic objects" we make in this study, we do not determine exactly which signal strength would be needed for a detection. In the case of the GC, broadly the signal strength needed for detection corresponds to the level advocated to explain the GC excess from dark matter annihilation, which for a 30 GeV—100 GeV dark matter particle is around 10^{-26} cm^3/ sec [11–14].

ACKNOWLEDGMENTS

This material is based upon work supported in part by the National Science Foundation Graduate Research Fellowship under Grant No. DGE-1842400 to N. S. S. P. is partly supported by the U.S. Department of Energy Grant No. de-sc0010107.

[1] P. A. Zyla *et al.* (Particle Data Group), Review of particle physics, Prog. Theor. Exp. Phys. **2020**, 083C01 (2020).
[2] S. Profumo, Dark matter indirect detection, EPJ Web Conf. **234**, 01014 (2020).
[3] T. R. Slatyer, TASI lectures on indirect detection of dark matter, arXiv:1710.05137.
[4] L. E. Strigari, dark matter in dwarf spheroidal galaxies and indirect detection: A review, Rep. Prog. Phys. **81**, 056901 (2018).
[5] A. Do, M. Duong, A. McDaniel, C. O'Connor, S. Profumo, J. Rafael, C. Sweeney, and W. Vera III, Cosmic-ray transport and gamma-ray emission in M31, arXiv:2012.14507.
[6] A. McDaniel, T. Jeltema, and S. Profumo, A multi-wavelength analysis of annihilating dark matter as the origin of the gamma-ray emission from M31, Phys. Rev. D **97**, 103021 (2018).
[7] S. Profumo and L. Ubaldi, Cosmic ray-dark matter scattering: A new signature of (asymmetric) dark matter in the gamma ray sky, J. Cosmol. Astropart. Phys. 08 (2011) 020.
[8] E. Board, N. Bozorgnia, L. E. Strigari, R. J. J. Grand, A. Fattahi, C. S. Frenk, F. Marinacci, and J. F. Navarro, Velocity-dependent J-factors for annihilation radiation from cosmological simulations, arXiv:2101.06284.
[9] L. Goodenough and D. Hooper, Possible evidence for dark matter annihilation in the inner Milky Way from the fermi gamma ray space telescope, arXiv:0910.2998.
[10] V. Vitale and A. Morselli, Indirect search for dark matter from the center of the Milky Way with the fermi-large area telescope, arXiv:0912.3828.
[11] D. Hooper and L. Goodenough, Dark matter annihilation in the galactic center as seen by the fermi gamma ray space telescope, Phys. Lett. B **697**, 412 (2011).
[12] T. Daylan, D. P. Finkbeiner, D. Hooper, T. Linden, S. K. N. Portillo, N. L. Rodd, and T. R. Slatyer, The characterization of the gamma-ray signal from the central Milky Way: A compelling case for annihilating dark matter, Phys. Dark Universe **12**, 1 (2016).
[13] T. F.-L. Collaboration, Fermi-LAT observations of high-energy gamma-ray emission toward the galactic center, Astrophys. J. **819**, 44 (2016).
[14] K. N. Abazajian, N. Canac, S. Horiuchi, and M. Kaplinghat, Astrophysical and dark matter interpretations of extended gamma-ray emission from the galactic center, Phys. Rev. D **90**, 023526 (2014).
[15] M. D. Mauro, X. Hou, C. Eckner, G. Zaharijas, and E. Charles, Search for γ-ray emission from dark matter particle interactions from the Andromeda and Triangulum galaxies with the Fermi large area telescope, Phys. Rev. D **99**, 123027 (2019).
[16] L. Feng, Z. Li, M. Su, P.-H. T. Tam, and Y. Chen, Searching for GeV gamma-ray emission from the bulge of M31, Res. Astron. Astrophys. **19**, 046 (2019).
[17] F.-L. Collaboration, Searching for Dark Matter Annihilation from Milky Way Dwarf Spheroidal Galaxies with Six Years of Fermi-LAT Data, Phys. Rev. Lett. **115**, 231301 (2015).
[18] A. A. Abdo *et al.*, Observations of Milky Way dwarf spheroidal galaxies with the Fermi-LAT detector and constraints on dark matter models, Astrophys. J. **712**, 147 (2010).
[19] J. Kumar and D. Marfatia, Matrix element analyses of dark matter scattering and annihilation, Phys. Rev. D **88**, 014035 (2013).
[20] F. Giacchino, L. Lopez-Honorez, and M. H. G. Tytgat, Scalar dark matter models with significant internal bremsstrahlung, J. Cosmol. Astropart. Phys. 10 (2013) 025.
[21] C. Han, H. M. Lee, M. Park, and V. Sanz, The diphoton resonance as a gravity mediator of dark matter, Phys. Lett. B **755**, 371 (2016).

[22] J. Kopp, J. Liu, T. R. Slatyer, X.-P. Wang, and W. Xue, Impeded dark matter, J. High Energy Phys. 12 (2016) 033.
[23] J. F. Navarro, C. S. Frenk, and S. D. M. White, A Universal density profile from hierarchical clustering, Astrophys. J. **490**, 493 (1997).
[24] L. Bergstrom and D. Hooper, Dark matter and gamma-rays from draco: Magic, glast and cactus, Phys. Rev. D **73**, 063510 (2006).
[25] A. Burkert, The structure of dark matter haloes in dwarf galaxies, Astrophys. J. **447**, L25 (1995).
[26] N. Klop, F. Zandanel, K. Hayashi, and S. Ando, Impact of axisymmetric mass models for dwarf spheroidal galaxies on indirect dark matter searches, Phys. Rev. D **95**, 123012 (2017).
[27] A. Drlica-Wagner, Search for gamma-ray emission from des dwarf spheroidal galaxy candidates with Fermi-LAT data, Astrophys. J. Lett. **809**, L4 (2015).
[28] C. Karwin, S. Murgia, I. Moskalenko, S. Fillingham, A.-K. Burns, and M. Fieg, Dark matter interpretation of the Fermi-LAT observations toward the outer halo of M31, Phys. Rev. D **103**, 023027 (2021).
[29] T. F. L. Collaboration, A. A. Abdo, D. E. Harris, F. Massaro, and L. Stawarz, Fermi large area telescope gamma-ray detection of the radio galaxy M87, Astrophys. J. **707**, 55 (2009).
[30] R. Bartels, S. Krishnamurthy, and C. Weniger, Strong Support for the Millisecond Pulsar Origin of the Galactic Center GeV Excess, Phys. Rev. Lett. **116**, 051102 (2016).
[31] D. Hooper and T. Linden, millisecond pulsars, TeV halos, and implications for the galactic center gamma-ray excess, Phys. Rev. D **98**, 043005 (2018).
[32] A. X. Gonzalez-Morales, S. Profumo, and F. S. Queiroz, Effect of black holes in local dwarf spheroidal galaxies on gamma-ray constraints on dark matter annihilation, Phys. Rev. D **90**, 103508 (2014).
[33] M. Ackermann *et al.* (Fermi-LAT Collaboration), Fermi-LAT observations of the diffuse gamma-ray emission: Implications for cosmic rays and the interstellar medium, Astrophys. J. **750**, 3 (2012).
[34] A. Albert *et al.*, Searching for dark matter annihilation in recently discovered Milky Way satellites with Fermi-LAT, Astrophys. J. **834**, 110 (2017).
[35] S. D. Hunter, P. F. Bloser, G. O. Depaola, M. P. Dion, G. A. DeNolfo, A. R. Hanu, M. L. Iparraguirre, J. Legere, M. L. McConnell, S. F. Nowicki, J. M. Ryan, S. Son, and F. W. Stecker, A pair production telescope for medium-energy gamma-ray polarimetry, Astropart. Phys. **59**, 18 (2014).
[36] R. K. Leane and T. R. Slatyer, Dark Matter Strikes Back at the Galactic Center, Phys. Rev. Lett. **123**, 241101 (2019).
[37] J. Shelton, S. L. Shapiro, and B. D. Fields, A Black Hole Window into p-Wave Dark Matter Annihilation, Phys. Rev. Lett. **115**, 231302 (2015).
[38] C. Johnson, R. Caputo, C. Karwin, S. Murgia, S. Ritz, and J. Shelton, Search for gamma-ray emission from p-wave dark matter annihilation in the galactic center, Phys. Rev. D **99**, 103007 (2019).
[39] M. A. Amin and T. Wizansky, Relativistic dark matter at the galactic center, Phys. Rev. D **77**, 123510 (2008).
[40] L. M. Widrow, Distribution functions for cuspy dark matter density profiles, Astrophys. J. Suppl. Ser. **131**, 39 (2000).
[41] K. A. Oman, J. F. Navarro, A. Fattahi, C. S. Frenk, T. Sawala, S. D. M. White, R. Bower, R. A. Crain, M. Furlong, M. Schaller, J. Schaye, and T. Theuns, The unexpected diversity of dwarf galaxy rotation curves, Mon. Not. R. Astron. Soc. **452**, 3650 (2015).